Available online at www.sciencedirect.com
ScienceDirect
Geochimica et Cosmochimica Acta 72 (2008) 1570–1582
Geochimica et Cosmochimica Acta
www.elsevier.com/locate/gca

Environmental and diagenetic variations in carbonate associated sulfate: An investigation of CAS in the Lower Triassic of the western USA

Pedro J. Marenco [a,*], Frank A. Corsetti [a], Alan J. Kaufman [b], David J. Bottjer [a]

[a] Department of Earth Sciences, University of Southern California, CA, USA
[b] Departments of Geology and Earth System Science Interdisciplinary Center, University of Maryland, MD, USA

Received 26 February 2007; accepted in revised form 23 October 2007; available online 26 January 2008

Abstract

An integrated stable isotope, elemental and petrographic analysis of Early Triassic (Spathian) carbonates and evaporites along a proximal to deep environmental transect reveals significant variations in $\delta^{34}S$ composition of carbonate associated sulfate (CAS). The variations in the $\delta^{34}S$ of CAS are strongly correlated with the Ca/Mg composition of carbonates, suggesting that the variations are driven by the degree of dolomitization. The $\delta^{34}S$ of dolostones and evaporites are similar to one another and exhibit lower $\delta^{34}S$ values than limestones from all localities.

Three hypotheses may explain the differences in $\delta^{34}S$ between proximal dolostones/evaporites and inner/middle shelf limestones: (1) limestones experienced anaerobic sulfate reduction and subsequent incorporation of ^{34}S-enriched sulfate into CAS during diagenesis, while dolostones did not—this is unlikely because of the lack of correlation between $\delta^{34}S_{CAS}$ and TOC, as well as other indicators of diagenesis, (2) dolomitization controlled the $\delta^{34}S_{CAS}$ in proximal paleoenvironments, where the source of the ^{34}S depleted fluids was either continentally-derived or the result of Rayleigh distillation during evaporite formation, and (3) a $\delta^{34}S$ depth gradient existed during the Early Triassic such that limestones formed in distal waters are more enriched in ^{34}S versus evaporites and dolostones formed in proximal settings—we do not favor this hypothesis because the strong correlation between Ca/Mg and $\delta^{34}S_{CAS}$ implies that dolomitization controls the $\delta^{34}S_{CAS}$ in these samples. Results from subtidal, well-preserved (non-dolomitized) limestones suggest that the $\delta^{34}S$ of Spathian seawater sulfate may have been heavier than previously suggested from analyses of evaporite deposits alone.

1. INTRODUCTION

The sulfur isotopic composition of seawater sulfate in ancient rocks can be an important indicator of evolving redox conditions in the ocean–atmosphere system (e.g., Claypool et al., 1980). The distribution of sulfate-bearing evaporite minerals, the most commonly used source of ancient sulfate for analysis, is sporadic in time and space. Evaporites are often deposited in restricted shallow-marine settings and therefore may not be representative of the open ocean. Evaporites are rare during the Precambrian and lack the age-diagnostic fossils that are used for correlation in Phanerozoic strata. Consequently, evaporite-based studies may be of limited value in the study of long-term atmospheric and oceanographic trends that may have had important consequences for the history of life. Marine barites have been used as well (Paytan et al., 1998), but it is not clear that they occur in enough abundance in shallow-marine settings to be useful in the ancient rock record.

It has been well documented that trace amounts of seawater sulfate are incorporated into the calcium-carbonate lattice of carbonate minerals (Kaplan et al., 1963; Mekhtiy-

* Corresponding author. Address: Department of Earth Sciences, University of California at Riverside, 1432 Geology, Riverside, CA 92521 0423, USA.
E-mail address: marenco@ucr.edu (P.J. Marenco).

0016-7037/$ - see front matter © 2008 Elsevier Ltd. All rights reserved.
doi:10.1016/j.gca.2007.10.033

eva, 1974; Burdett et al., 1989). Because the record of ancient carbonates is more complete than the record of marine evaporites, the analysis of carbonate associated sulfate (CAS) is becoming an important tool for studying ancient ocean–atmosphere chemistry. Sulfur isotopic analysis of CAS has been used for a variety of geochemical studies on recent and ancient carbonates (Kaiho et al., 2001; Kampschulte et al., 2001; Hurtgen et al., 2002; Kah et al., 2004; Kampschulte and Strauss, 2004; Newton et al., 2004; Gellatly and Lyons, 2005; Riccardi et al., 2006). Kaplan et al. (1963) first reported $\delta^{34}S$ compositions comparable to that of seawater from sulfate bound in modern mollusc shells. Mekhtiyeva (1974) used the $\delta^{34}S_{CAS}$ of fossil mollusc shells as an indicator of geochemical conditions in ancient basins. Burdett et al. (1989) further studied the $\delta^{34}S$ composition of CAS in modern mollusc shells and foraminiferal tests from the Miocene to the Recent, and reported that $\delta^{34}S_{CAS}$ in both forms was similar to that of modern seawater and the evaporite sulfate curve. Lyons et al. (2004) demonstrated that the $\delta^{34}S$ of CAS in recent micrite sediments agrees with the $\delta^{34}S$ of modern seawater sulfate.

Although CAS in recent sediments has been shown to agree with modern seawater sulfate, the fidelity of the CAS signals in rocks that have undergone variable degrees of alteration (including dolomitization) remains uncertain, and diagenetic studies are warranted. One way to test the CAS method in ancient rocks is to compare CAS with sulfur isotopic data from interbedded marine sulfates. One such test revealed that $\delta^{34}S_{CAS}$ from Mesoproterozoic (1.2 Ga) dolostones agreed closely (+3‰ to 5‰) with $\delta^{34}S$ of associated evaporite deposits (Kah et al., 2004). Hurtgen et al. (2006) observed ^{34}S-enriched CAS values in dolostone units relative to underlying limestone units following Neoproterozoic glacial deposits. However, a systematic, along-transect investigation of CAS in coeval limestones and dolostones, along with interbedded evaporite $\delta^{34}S$ has yet to be reported in younger rocks.

The present study is an investigation of the CAS method using interbedded carbonates (limestones and dolostones) and evaporites from Lower Triassic rocks across a spectrum of well-constrained shallow-marine paleoenvironments. The goal of this study is to investigate the dynamics of CAS abundance and isotope composition with changing environment and diagenetic grade. The results of a detailed petrographic, isotopic (sulfur, carbon, oxygen, and strontium), and elemental (Ca, Mg, Mn, Sr, Fe, and organic C) analysis of interbedded carbonate and evaporite units are reported here in order to investigate the veracity of the CAS record across an onshore–offshore transect in a well-constrained depositional system.

2. GEOLOGIC SETTING

The Lower-Middle Triassic (McKee, 1954) Moenkopi Formation was chosen for this study because it contains interbedded carbonate and sulfate deposits in nearshore localities and carbonate-rich, non-restricted inner and middle shelf deposits in the offshore localities. The Moenkopi Formation consists of siliciclastic and carbonate strata deposited on a westward-dipping, distally-steepened ramp (Blakey, 1974). The Virgin Limestone Member (hereafter referred to as the Virgin Limestone) of the Moenkopi Formation represents a marine transgression and subsequent regression that fostered the deposition of carbonate and siliciclastic sediments over what is now southern Nevada, northern Arizona, and southern Utah (e.g., Poborski, 1954). The occurrence of the ammonoid *Tirolites* in the Virgin Limestone indicates a latest Early Triassic (Spathian) age (McKee, 1954; Poborski, 1954), which is corroborated by $^{87}Sr/^{86}Sr$ chemostratigraphy, as discussed below.

In order to investigate the abundance and $\delta^{34}S$ composition of CAS with changing environment and diagenetic grade, we systematically sampled carbonates and bedded evaporites along an environmental transect within three Virgin Limestone localities—Beyond Lost Cabin (BLC), Blue Diamond (BD), and Rainbow Garden (RG) (Fig. 1). The three localities are approximately equally spaced when shortening along the Wilson Cliffs and Keystone thrusts (greater than 20 km displacement; Burchfiel et al., 1997) is restored to the original configuration.

The Beyond Lost Cabin locality, the most distal of the three, is located in the Spring Mountains east of the town of Pahrump, Nevada, approximately 2 km southeast of Lost Cabin Springs (Fig. 1). At the Beyond Lost Cabin locality, the Moenkopi Formation measures 224 m. The base of the section was taken to be the first carbonate unit above the unconformity with Permian strata. The initial transgression above the unconformity is followed by a shallowing interval of interbedded bioclastic limestone and calcareous shale that increase in grain-size upward for 85 m (Fig. 2). Following a major flooding surface at 85 m the lithofacies then shallow considerably to the top of the section, punctuated by another major flooding surface at 152 m and an increase in shallow-water sedimentary structures such as herring-bone cross stratification, flaser bedding and oolites.

The Blue Diamond locality is located southwest of Las Vegas (Fig. 1). The Virgin Limestone is approximately 140 m thick at this site (e.g., Larson, 1966). The top 40 m

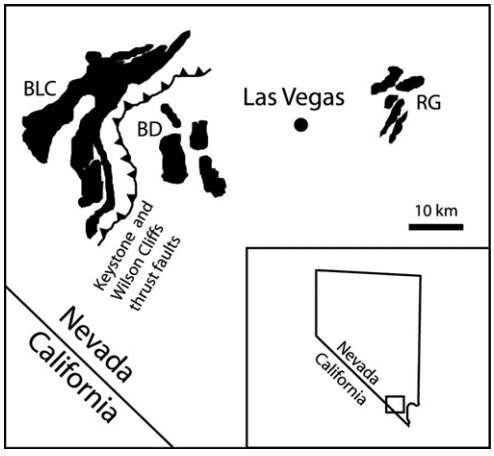

Fig. 1. Map showing the localities used in this study: Beyond Lost Cabin (BLC), Blue Diamond (BD), Rainbow Garden (RG). Dark areas represent outcrops of Moenkopi Formation strata. Modified from Bissell (1970).

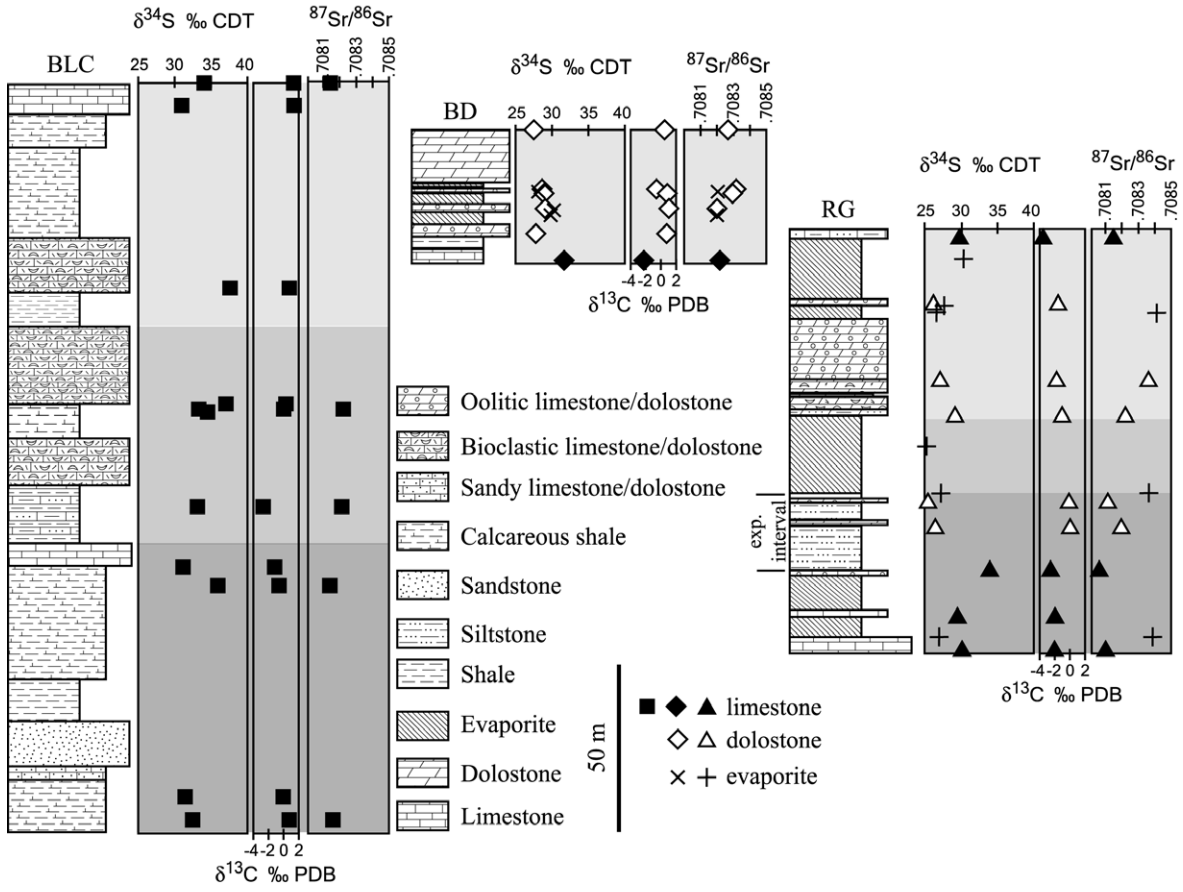

Fig. 2. Stratigraphic columns showing isotopic results and correlation of major flooding surfaces (lower boundaries of shaded regions) between the two complete localities.

(containing interbedded limestone and evaporites; e.g., Bissell, 1970) were accessible when this study was underway (Fig. 2).

The Rainbow Garden locality, the most proximal of the three, is located near Frenchman Mountain on the east side of Las Vegas (Fig. 1). The base of the Virgin Limestone at Rainbow Garden consists of bivalve- and microgastropod-rich, ledge-forming carbonate with thin-bedded evaporites (10 cm–1 m). The lithofacies record a shallowing-upward trend from the base, culminating in an exposure interval typified by poorly lithified red silt and mud beginning at 20 m (Fig. 2). Two thin (10 cm) white oolite beds are found within the exposure interval, approximately 7 m apart. Above the exposure interval, a thick (~20 m) evaporite interval is followed by an equally thick oolitic dolostone that represents a subsequent deepening of the lithofacies. A last prominent evaporite unit with minor carbonate marks a second shallowing and the final retreat of sea level at this locality.

High-resolution sequence stratigraphic correlations are difficult using outcrop data in mixed siliciclastic–carbonate successions. However, major flooding surfaces following shallowing intervals can be correlated between the two complete sections (Beyond Lost Cabin and Rainbow Gardens) and are represented in Fig. 2 by the bases of each of three shaded regions.

3. PREVIOUS RESULTS

The $\delta^{34}S$ of Moenkopi Formation bedded-sulfates has been previously reported by other researchers (Claypool et al., 1980; Wilgus, 1981). Previous $\delta^{34}S$ studies of Lower Triassic evaporites reveal an anomalous enrichment in the ^{34}S composition of Early Triassic ocean basins from around the world. Although there is a broad range of values (Fig. 3), most Spathian $\delta^{34}S$ values fall between +25‰ and +30‰ VCDT (e.g., Cortecci et al., 1981; Holser, 1984; Holser and Magaritz, 1987; Holser et al., 1988; Strauss, 1997) with a mean of +27‰ (Holser et al., 1988). Early Triassic $\delta^{34}S$ values are distinctly more positive than the rest of the Phanerozoic, with the exception of the Cambrian and Devonian periods (e.g., Cortecci et al., 1981; Holser, 1984; Holser and Magaritz, 1987; Strauss, 1997).

The Early Triassic strontium isotope record published by Korte et al. (2003) reveals a nearly monotonic rise in the $^{87}Sr/^{86}Sr$ composition of seawater during the Early Triassic; during the Spathian, seawater $^{87}Sr/^{86}Sr$ was between 0.7080 and 0.7082 (Fig. 4). The $\delta^{13}C_{carbonate}$ profile for the Early Triassic demonstrates that this stage was characterized by large fluctuations in the $\delta^{13}C$ composition of seawater carbonate (Baud et al., 1996; Payne et al., 2004; Corsetti et al., 2005). Spathian $\delta^{13}C_{carb}$ values appear to fall between −1‰ and +3‰ PDB—a range of ~4‰ (Payne et al., 2004).

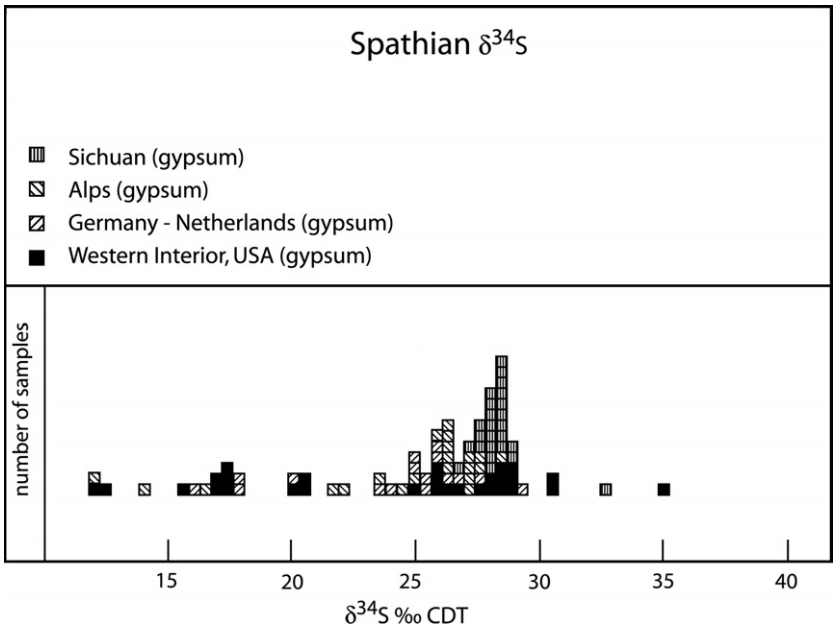

Fig. 3. Spathian $\delta^{34}S$ values. Modified from Holser (1984) and references therein.

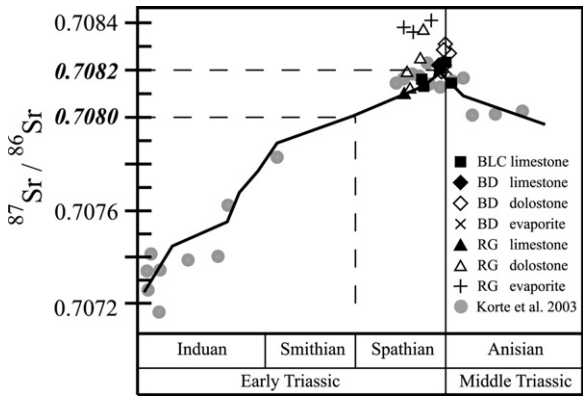

Fig. 4. Early Triassic strontium isotopes. Modified from Korte et al. (2003).

4. METHODS

4.1. Sampling and preparation

Visibly well-preserved samples (those with the least amount of visible veins and fractures) were preferentially collected from each locality. In the onshore localities (Rainbow Gardens and Blue Diamond), care was taken to collect carbonates in close proximity to bedded evaporites for the comparison studies outlined above. In the laboratory, carbonate samples for isotopic analyses were first prepared by trimming any obvious diagenetic phases, such as large veins. The samples were then cut into smaller pieces; one billet from each sample was used for thin sectioning and micro-drilling, the rest were powdered using a Rock Labs standard ring mill. The cut faces of evaporite samples were drilled for isotopic analysis.

4.2. Petrographic analysis and micro-drilling of carbonates

Detailed petrographic analysis was carried out on each sample in order to assess the effects of diagenesis. The petrographic analyses included staining (for a visual determination of mineralogy and iron content), cathodoluminescence, and the construction of a paragenetic sequence for each sample. Each sample was thin-sectioned and stained with Alizarin red S and potassium ferricyanide (Dickson, 1966). The staining was used to distinguish calcite from dolomite and to indicate Fe-rich carbonate phases. The luminescence of each sample was compared to that of other samples from the same study and ranked on a scale of 1-9 (where 1 is dark red to black in color and 9 is bright orange). This combined petrographic approach was used to determine the least altered carbonate phases for micro-drilling directly on the thin-section billet. Micro-drilled powders were used for carbon, oxygen, and strontium isotopic analyses, as well as manganese, strontium, calcium, magnesium, and iron elemental analyses.

4.3. Extraction of carbonate associated sulfate

The extractions of CAS in this study were a modification of the method of Burdett et al. (1989). Approximately 150–300 g of carbonate powder were subjected to two consecutive 8-h washes in 2 l of 18.2 MΩ distilled water. After gravitational settling, the supernate was aspirated from the residual powder. The purpose of the washes was to dissolve and remove any soluble sulfur phases, including pyrite oxidized on the outcrop and minor evaporite inclusions. The samples were then washed for 8 h in a solution consisting of 105 ml of 6% NaOCl (bleach) added to 1895 ml of DDI water. The supernate was then aspirated. The bleach step was designed to oxidize organic matter and hence re-

move any organic sulfur present in the sample. The samples were then subjected to two additional washes in DDI water to dilute and remove any residual bleach.

The samples were then dissolved using 3 M HCl. The amount of HCl to be added was determined using the stoichiometric ratios necessitated by the starting sample mass (assuming the sample was pure carbonate); the purpose of this calculation was to dissolve all of the carbonate while minimizing the risk of dissolving any remaining sulfide phases that may oxidize at lower pH. The samples were allowed to dissolve for 8 h. The samples were then filtered through a series of filter papers, ultimately through a 0.45 μm membrane filter, to remove insoluble particulate matter. The insolubles were then weighed; the mass of insolubles was then subtracted from the starting mass of sample in order to determine the mass of carbonate dissolved.

An aliquot of 50–100 ml (depending on starting mass of sample) of a 30% $BaCl_2$ solution (300 g of anhydrous $BaCl_2$ powder dissolved into 1000 ml of DDIW) was then added to each sample after heating to sub-boiling temperature. Because $BaSO_4$ (barite) is very insoluble, ionic exchange occurs if any SO_4^{2-} is present in the sample and barite is precipitated. The samples were left for three days to ensure that any sulfate present had precipitated as barite. The barite was then filtered from the sample with a 0.45 μm membrane. The filters were then dried and weighed. The mass of barite precipitated was used to calculate the amount of CAS in the sample, taking the mass of insoluble residue into account. Based on replicate samples, the uncertainty in the CAS abundance measurement is ~8%.

4.4. Isotopic analyses

4.4.1. Sulfur

A Eurovector elemental analyzer (EA) was used for on-line combustion of barite and evaporite powders and the separation of SO_2 on-line to a GV Isoprime mass spectrometer for $^{34}S/^{32}S$ analyses following the procedures outlined by (Grassineau et al., 2001). The effluent from the EA is introduced in a flow of He (80–120 ml/min) to the IRMS through a SGE splitter valve that controls the variable open split. Timed pulses of SO_2 reference gas (99.9% purity, ~3 nA) are introduced at the beginning of the run using an injector connected to the IRMS with a fixed open ratio split. The isotope ratios of reference and sample peaks are determined by monitoring ion beam intensities relative to background values.

Prepared samples (~100 μg) are accurately weighed and folded into small tin cups that are sequentially dropped with a pulsed O_2 purge of 12 ml into a catalytic combustion furnace operating at 1030 °C. The frosted quartz reaction tube is packed with granular tungstic oxide on alumina ($WO_3 + Al_2O_3$) and high purity reduced copper wire for quantitative oxidation and O_2 resorption. Water is removed from the combustion products with a 10-cm magnesium perchlorate column, and the SO_2 is separated from other gases with a 0.8-m PTFE GC column packed with Porapak 50–80 mesh heated to 90 °C. The cycle time for these analyses was 210 s with reference gas injection as a 30-s pulse beginning at 20 s. Sample SO_2 pulses begin at 110 s and return to baseline values between 150 and 180 s, depending on sample size and column conditions. Isotope ratios are determined by comparing integrated peak areas of *m/z* 66 and 64 for the reference and sample SO_2 pulses, relative to the baseline of $\sim 1 \times 10^{-11}$A. Isotopic results are expressed in the δ notation as per mil (‰) deviations from the VCDT standard. One sigma uncertainties of these measurements (±0.3‰ or better) were determined by multiple analysis of a standard barite (NBS 127) interspersed with the samples.

4.4.2. Carbon and oxygen

Carbonate powders were reacted for 10 min at 90 °C with anhydrous H_3PO_4 with a Multiprep inlet system in-line with a water trap and dual inlet GV Isoprime gas source mass spectrometer in the Stable Isotope Facility of the University of Maryland Geochemical Laboratories. Isotopic results are expressed in the standard δ notation as per-mil (‰) deviations from the VPDB international standard. Uncertainties determined by multiple measurements of a laboratory standard carbonate (calibrated to NBS-19) during each run of samples were better than 0.05‰ for both C and O isotopes.

4.4.3. Strontium

Micro-drilled carbonate and evaporite powders were weighed and placed in cleaned micro-centrifuge tubes, then pre-treated for 2 h with 0.5 M ammonium hydroxide (~8.2 pH) to leach loosely bound Sr from clay and other silicate surfaces (Montanez et al., 1996). Samples were centrifuged and aspirated between each of three leaches and the final addition of 0.5 M acetic acid, which was allowed to sit for 12 h. Strontium was isolated and purified by passing the solution through a small Sr-spec© loaded column with successive washes of 3 and 7 M HNO_3 (primarily to remove Ca from the solution), and then a wash of 0.05 M HNO_3 (to elute purified Sr), which was collected in small Teflon© beakers. This aliquot was dried to a spot, re-dissolved in ~2 μl of 3 M HNO_3, and then ~1 μl was loaded carefully on the middle of a pre-baked Re filament. The Sr spot was mixed with ~0.8 μl of TaO in water and then dried, allowing the filament to briefly glow slightly in air after about 5 min of progressive heating.

Samples were analyzed on a VG 54 multi-collector thermal ionization mass spectrometer through the measurements of masses 84 through 88 in dynamic mode. Strontium isotope ratios were collected for instrumental mass fractionation based on an exponential law by monitoring systematic changes in $^{86}Sr/^{84}Sr$. Multiple NBS-987 Sr isotope standard solutions measured over the period of sample analyses yielded an average of 0.710245 ± 0.000011 (2σ).

4.5. Elemental analyses

Approximately 1.5 mg of micro-drilled powdered sample were acidified with 1 ml of 10% nitric acid and analyzed with a JY Ultima-C ICP-AES with Polychronometer. Samples were analyzed with interspersed standards of known concentrations to correct for analytical drift. Replicate analyses of standards produced results within 0.7%, 1.5%,

1.4%, 2.0%, and 11% of known values for Mn, Sr, Mg, Ca, and Fe, respectively.

Approximately 7–14 mg of bulk powdered sample for organic carbon abundance were weighed in silver boats and dissolved overnight by exposure to HCl vapor in a sealed dessicator. Residues were then reweighed and analyzed with a CE Elantech CHNS analyzer. Replicate analyses of standards produced results within 1% of known values.

5. RESULTS

The results of the geochemical and petrographic analyses are given in Table 1, as well as Fig. 2, and are discussed in detail below.

5.1. Petrographic analysis

The samples from Beyond Lost Cabin (BLC) are predominantly bioclastic wackestones. Petrographic analysis of the stained thin sections demonstrates the presence of iron rich phases and the general absence of dolomite in the samples. In terms of relative cathodoluminescence, the BLC samples had medium to high levels of brightness (orange, levels 5–7).

Carbonate samples from Blue Diamond (BD) include micrites, bioclastic micrites and oolites. The staining of sample BD-0 indicated the predominance of Fe-poor calcite in the bioclasts and much of the micritic matrix. The rest of the samples from this locality were predominantly dolomite. Some of the dolostones exhibit primary fabric retention (mimetic dolomitization). Formerly-gypsum inclusions are present but rare in Blue Diamond dolostones. Compared to the other samples in this study, the Blue Diamond thin sections exhibit low to moderate levels of cathodoluminescence (dark red to orange, levels 1–6.)

The Rainbow Garden (RG) carbonate samples are either oolite grainstones or oolitic and bioclastic micrites. The oolites were largely grain supported with 50–70% porosity. Staining indicated that both Fe-poor calcite and dolomite are present in the section. The samples from the lower 25 m of the section are predominantly calcitic, with some limestone samples exhibiting significant dolomitization (as indicated by staining). Most of the rest of the samples are predominantly dolomite with minor Fe-rich calcite. Gypsum and formerly-gypsum inclusions are present but rare in the dolostones. Much of this section has experienced pervasive dolomitization, although some of the samples retain their depositional fabrics. Dolomite rhombs, when visible, vary between less than 10 and 35 μm. Compared to the other samples in this study, the thin sections from Rainbow Garden exhibit anywhere from low to very high cathodoluminescence (from dark red to bright orange, levels 2–9). The two oolite samples found within the exposure interval (RG-38 and RG-45) are the most cathodoluminescent samples of this study (bright orange, levels 8 and 9).

5.2. Elemental analyses

The Ca/Mg ratios based on quantitative chemical analysis reflect the results of the thin-section staining. Samples from the Beyond Lost Cabin locality are limestone, whereas samples from Blue Diamond and Rainbow Garden include limestone and dolostone.

Samples from Beyond Lost Cabin contained the most Fe of all limestone samples in this study (Fig. 5A). The limestones from Rainbow Garden contain the least Fe, with the one limestone sample from Blue Diamond exhibiting an intermediate Fe content. However, as a whole, dolostone samples exhibit the highest Fe concentrations, especially those from the Blue Diamond locality. Samples with the greatest luminescence are also those that contain the most Mn (Table 1), a know luminescence activator, which are highlighted by samples from the two exposure intervals at Rainbow Garden. The least luminescent samples (those from Blue Diamond) exhibit Mn concentrations comparable with other samples, but exhibit higher Fe concentrations, a known luminescence inhibitor.

Most of the samples exhibit Mn/Sr values close to or less than 1 (Table 1). Samples with higher Mn/Sr values (e.g., the two exposure interval dolostone samples from Rainbow Garden) exhibit comparable Sr concentrations to other samples but contain much higher concentrations of Mn.

The $[SO_4]_{CAS}$ results show a variation with Ca/Mg and with locality (Fig. 5B). Samples with the highest CAS concentrations exhibit the lowest Ca/Mg values. Limestone samples from the three localities exhibit the lowest CAS concentrations (~20 to ~700 ppm with only one sample from Rainbow Garden exhibiting a higher value of ~2900 ppm). Partially dolomitized limestones from Rainbow Garden exhibit intermediate CAS concentrations (~700 to ~900 ppm). Dolostone samples from Blue Diamond and Rainbow Garden exhibit the highest CAS concentrations (~700 to ~6800 ppm). As a whole, samples from Blue Diamond and Rainbow Garden contain more CAS than samples from Beyond Lost Cabin.

Most samples exhibit organic carbon abundances between ~0.05 and 0.15 wt% (Table 1 and Fig. 6A). Two samples exhibit higher organic carbon abundance, a Blue Diamond dolostone (0.27%) and a Beyond Lost Cabin limestone (0.38%).

5.3. Isotopic analyses

5.3.1. Strontium

About half of the carbonate samples in this study fall within the range of expected values for the Spathian (between 0.7080 and 0.7082; Figs. 2 and 6B). The remainder of the samples exhibit only slightly more radiogenic strontium isotope values (the highest being 0.70832). Notably, the most radiogenic $^{87}Sr/^{86}Sr$ values are from dolostone samples taken from the Blue Diamond locality; however, there is no discernable trend between strontium isotopes and Ca/Mg. The evaporite samples from Blue Diamond exhibit $^{87}Sr/^{86}Sr$ values in close agreement to closely associated dolostone samples (~0.7082) whereas evaporite samples from Rainbow Garden exhibit values that are more radiogenic (~0.7084) than closely associated dolostones.

Table 1
Geochemical and petrographic results

Sample	$\delta^{34}S$ (‰) VCDT	$^{87}Sr/^{86}Sr$	$\delta^{13}C$ (‰) VPDB	$\delta^{18}O$ (‰) VPDB	$[SO_4]$ (ppm)	[Mn] (ppm)	[Sr] (ppm)	[Mg] (ppm)	[Ca] (ppm)	[Fe] (ppm)	C_{org} (wt%)	CL	Lithology
BLC-224	34.12	0.70814	1.19	−7.35	24	190	572	2752	385039	1210	.073	5	Limestone
BLC-218	30.93		1.31	−7.20	94	257	333	2353	372202	1296	.126		Limestone
BLC-163	37.54		0.65	−7.73	267	248	638	3180	379146	1261			Limestone
BLC-128	36.99		0.26	−7.38	50	214	1161	3696	353366	2079			Limestone
BLC-127	33.12	0.70823	−0.02	−7.66	439	329	515	4780	375204	2078		7	Limestone
BLC-97.5	33.06	0.70821	−2.69	−8.64	291	1480	410	3352	347988	1959	.056	7	Limestone
BLC-80	31.04		−1.36	−8.10	371	436	370	3053	370278	2039			Limestone
BLC-74	35.89	0.70813	−0.59	−7.61	401	226	648	4371	370054	1636	.107	7	Limestone
BLC-11.2	31.51		−0.07	−7.25	303	552	671	3619	343878	3172			Limestone
BLC-3.5	32.30	0.70816	0.65	−7.60	308	177	1832	3914	381105	1456	.380	6	Limestone
BD-40	27.42	0.70827	0.51	−5.05	735	279	197	101512	205017	3482	.075	5	Dolostone
BD-22.5	28.55	0.70832	−0.51	−5.40	3625	287	517	73543	263063	3446	.062	5	Dolostone
BD-21.5	28.11	0.70820											Evaporite
BD-21	28.67	0.70829	0.80	−4.54	6334	229	550	108749	193818	3980		4	Dolostone
BD-16.5	28.98	0.70819	0.99	−4.20	6732	278	30575	101287	183838	4622	.273	1	Dolostone
BD-16	30.26												Evaporite
BD-14.5	29.88	0.70819											Evaporite
BD-9	27.78		0.69	−2.93	6001	359	543	107064	201598	3783	.045	6	Dolostone
BD-0	31.68	0.70822	−2.34	−7.48	725	318	356	4395	388979	1457	.081	6	Limestone
RG-124	29.62	0.70820	−3.63	−6.50	721	181	170	20122	377022	1006	.078	5	Limestone
RG-118	30.31												Evaporite
RG-104.05	26.34		−1.64	−4.96	6081	178	289	104196	204963	2039		5	Dolostone
RG-104	27.83												Evaporite
RG-102	26.65	0.70841											Evaporite
RG-82	27.11	0.70837	−1.84	−5.40	2186	297	262	69439	247465	4357		7	Dolostone
RG-71	29.10	0.70825	−0.55	−4.52	1316	211	274	109528	208539	2822	.045	2	Dolostone
RG-62	25.04												Evaporite
RG-48	27.02	0.70836											Evaporite
RG-45	25.39	0.70812	−0.21	−4.15	5378	1650	232	103219	198712	2393	.064	9	Dolostone
RG-38	26.51	0.70819	−0.04	−4.62	5410	1316	182	101548	214969	1572		8	Dolostone
RG-25	33.93	0.70806	−2.65	−8.48	2864	132	4691	4656	388427	1002		3	Limestone
RG-11	29.55		−1.92	−7.70	875	167	188	20831	311523	1156		3	Limestone
RG-5	26.95	0.70838											Evaporite
RG-0	30.22	0.70804	−2.07	−7.99	789	133	167	8529	373688	565	.053	7	Limestone

CL refers to the degree of cathodoluminescence.

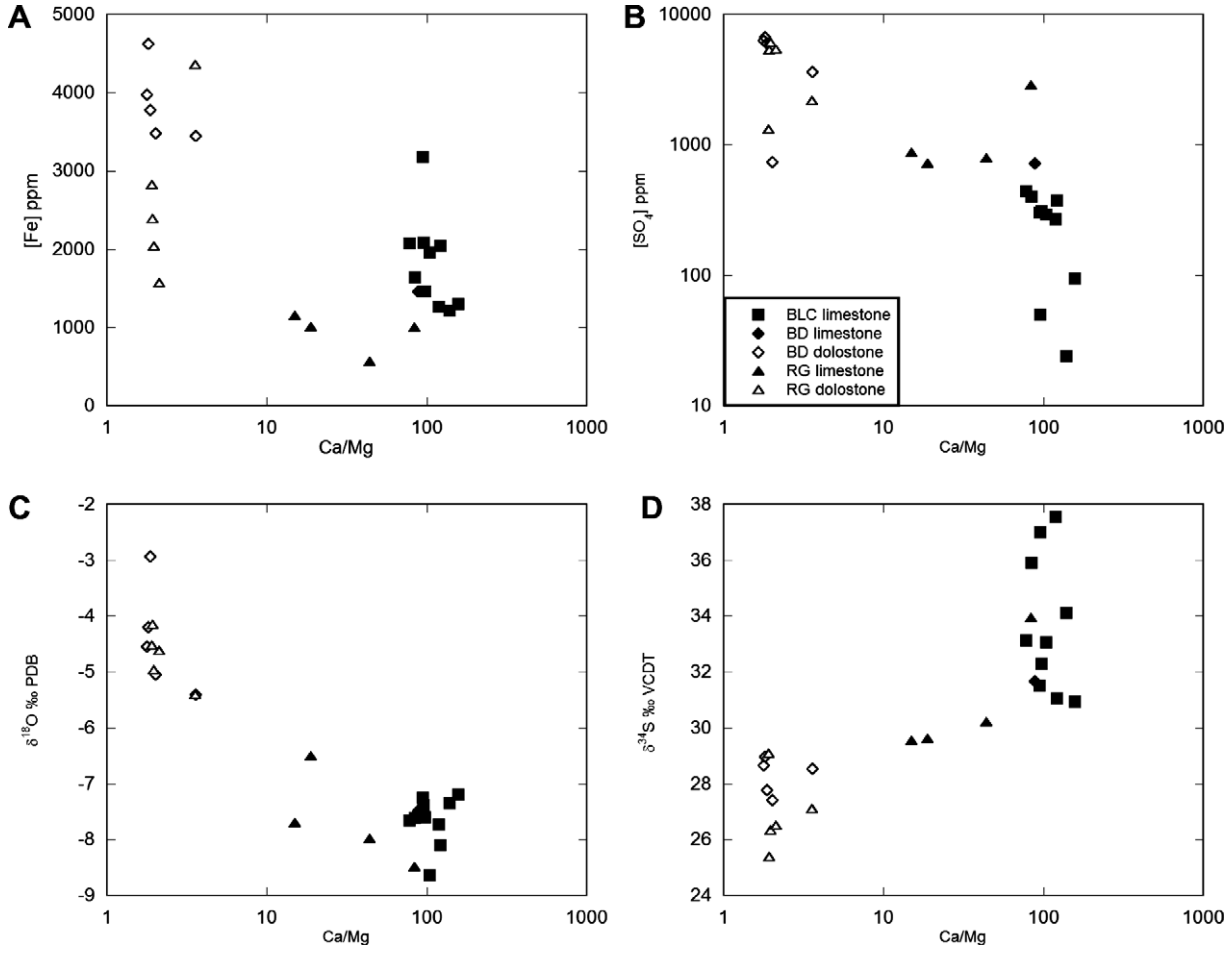

Fig. 5. Stable isotope and trace element cross plots versus Ca/Mg. Locality abbreviations are the same as in Fig. 1.

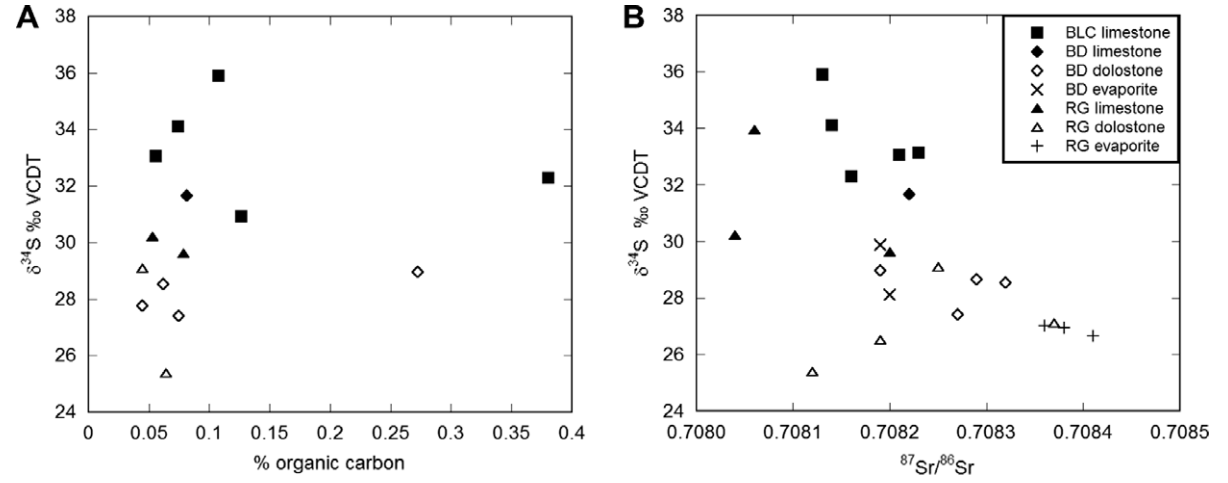

Fig. 6. $\delta^{34}S$ of evaporites and carbonates versus C_{org} and $^{87}Sr/^{86}Sr$.

5.3.2. Oxygen

The carbonates in this study exhibit a strong relationship between $\delta^{18}O$ and Ca/Mg compositions (Fig. 5C). Limestones from Beyond Lost Cabin and Blue Diamond exhibit the lowest oxygen isotope values (approximately −8.6‰ to −7.3‰ VPDB). Limestones with low Ca/Mg from Rainbow Garden exhibit intermediate oxygen isotope values (approximately −8‰ to −6.5‰). Dolostones from Blue Diamond and Rainbow Gardens exhibit the highest oxygen isotope values (approximately −5.4‰ to −2.9‰).

5.3.3. Carbon

The majority of samples in this study exhibit $\delta^{13}C_{carb}$ values within the range −3‰ to +1‰ VPDB (Fig. 2). Overall, the range of carbon isotope values in this study is about 2‰ more negative than results from Spathian-aged carbonates reported by Payne et al. (2004), but the range of values is approximately the same (~4‰). The carbon isotopic results from this study do not vary systematically with any of the other isotopic or trace elemental results.

5.3.4. Sulfur

The $\delta^{34}S$ values of both evaporites and CAS in this study fall between +25‰ and +38‰ VCDT. Interbedded evaporite and dolostone at Blue Diamond and Rainbow Garden show very close agreement (Figs. 2 and 6B). Differences between the $\delta^{34}S$ of interbedded evaporite and dolostone are between −0.4‰ and +1.6‰, which is comparable to the results from interbedded evaporite and dolostone reported for a Mesoproterozoic succession by Kah et al. (2004).

The results indicate a strong relationship between $\delta^{34}S_{CAS}$ and Ca/Mg compositions (Fig. 6D). Limestones from all three localities exhibit higher sulfur isotope values (approximately +31‰ to +38‰) than either evaporite or dolostone. Partially dolomitized limestone samples from Rainbow Garden exhibit intermediate $\delta^{34}S_{CAS}$ values (~+30‰), whereas dolostone samples from Blue Diamond and Rainbow Garden exhibit the lowest sulfur isotope values (approximately +25‰ to +29‰). The range of evaporite $\delta^{34}S$ values from Blue Diamond and Rainbow Garden is similar to the range of dolostone $\delta^{34}S$ values (+25‰ to +30‰; Fig. 6B).

There is also an apparent trend between $\delta^{34}S_{CAS}$ compositions and CAS concentrations (Table 1). The dolostone samples from Blue Diamond and Rainbow Garden with the lowest $\delta^{34}S$ values tend to have the highest CAS concentrations whereas the limestones from Beyond Lost Cabin with the highest $\delta^{34}S$ values tend to have the lowest CAS concentrations. Likewise, there is an apparent trend between $\delta^{34}S_{CAS}$ and $\delta^{18}O$ (Table 1). Limestones with the highest $\delta^{34}S_{CAS}$ values exhibit the lowest $\delta^{18}O$ values whereas dolostones with the lowest $\delta^{34}S_{CAS}$ values exhibit the highest $\delta^{18}O_{carb}$ values. However, there are no significant trends between $\delta^{34}S_{CAS}$ and Mn/Sr, $\delta^{34}S_{CAS}$ and [Fe], $\delta^{34}S_{CAS}$ and $\delta^{13}C_{carb}$, or $\delta^{34}S$ and $^{87}Sr/^{86}Sr$.

6. INTERPRETATIONS

The interpretations that follow are based on the assumption that our samples from the three Virgin Limestone localities are broadly time equivalent, as the biostratigraphy suggests. This assumption is strongly supported by the strontium isotope results that imply a Spathian-age for the three studied sections (Figs. 2 and 4). The results of the combined analyses reported here reveal significant variation in the $\delta^{34}S$ of CAS both within a given locality and among the three localities. A lack of correlation between the variations in $\delta^{34}S$ and indicators of diagenesis such as Mn/Sr and $^{87}Sr/^{86}Sr$ suggest that the CAS results cannot be simply ruled out as being "diagenetic" in origin. Rather, the strong correlation between $\delta^{34}S_{CAS}$ and Ca/Mg (Fig. 5D) suggests that dolomitization—a specific diagenetic process—played a prominent role in the observed $\delta^{34}S_{CAS}$ values. Trends could also be discerned between $\delta^{34}S_{CAS}$ and $[SO_4]_{CAS}$, and $\delta^{34}S_{CAS}$ and $\delta^{18}O_{carb}$; however, these trends are similarly driven by the degree of dolomitization (Fig. 5B and C).

Limestone samples exhibiting Ca/Mg values greater than 50 are interpreted here to be recording the least altered $\delta^{34}S_{sulfate}$ values, which range between +31‰ and +38‰ VCDT, a variation of 7‰; this entire range is represented by the samples from Beyond Lost Cabin. Therefore, we interpret the $\delta^{34}S_{CAS}$ results from Beyond Lost Cabin (Fig. 2) to best represent whole ocean $\delta^{34}S$ during the Spathian.

6.1. Hypothesis 1: Bacterial sulfate reduction during diagenesis

The ^{34}S-enrichment of the distal limestone samples relative to the more proximal dolostone samples could be explained by anaerobic sulfate reduction during diagenesis. However, the TOC data argue against diagenetic sulfate reduction and subsequent incorporation as CAS. A positive correlation between $\delta^{34}S$ and organic carbon abundance might indicate sufficient organic matter to fuel bacterial sulfate reduction. However, the samples contain vanishing small amounts of organic matter (~0.1 or less wt%), consistent with their position on a well-oxygenated carbonate platform. Alternatively, if organic carbon abundances were relatively uniform, yet showed a negative relationship with $\delta^{34}S$, then samples with lower organic carbon abundance and higher $\delta^{34}S$ could be interpreted to have undergone bacterial sulfate reduction, which would have resulted in a decrease in organic carbon content and an increase in $\delta^{34}S$. To the contrary, the organic carbon and $\delta^{34}S$ data show no trends (Fig. 6A) and therefore do not support the hypothesis that the limestones are ^{34}S-enriched because of sulfate reduction during diagenesis. Furthermore, the low Mn/Sr and marine Sr isotopic composition would suggest the samples are well-preserved.

6.2. Hypothesis 2: Influence of dolomitization on CAS

Fig. 5D reveals a clear trend between the degree of dolomitization and the $\delta^{34}S_{CAS}$, with the dolomitized samples recording $\delta^{34}S_{CAS}$ values much lower than the coeval limestones. The data fall into two main groups: the inner to middle shelf limestones with $\delta^{34}S_{CAS} \sim +31‰$ to +38‰ and the proximal dolostones plus evaporites with $\delta^{34}S$ values between +25‰ and +30‰ VCDT. Incompletely dolomitized samples record the intermediate $\delta^{34}S_{CAS}$in the aforementioned ranges. The stratigraphic co-occurrence of dolostone and evaporite suggests that, for the samples in this study, the dolomitization process was strongly facies-dependent, with the more proximal paleoenvironments experiencing a greater degree of dolomitization; this interpretation is supported by the lack of dolomitization in the most distal locality (Beyond Lost Cabin). Facies dependency might explain why the range of $\delta^{34}S_{evaporite}$ values

(+25‰ to +30‰ VCDT) and $\delta^{34}S_{dolostone}$ values (+25‰ to +29‰) show such strong overlap.

Dolomitization most likely occurred early in the study section. In thin section, some dolomitized samples show remarkable primary fabric retention of ooids (mimitic dolomitization, e.g., Corsetti et al., 2006). Where dolomite rhombs are visible, grain sizes are notably small, from less than 10 μm to about 30 μm in length. Although there are no distinct trends between $^{87}Sr/^{86}Sr$ and Ca/Mg, the fact that some dolostones record marine strontium isotope values (Figs. 2, 4, and 6B) makes it unlikely that dolomitization was a late diagenetic process.

It is possible that the $\delta^{34}S_{CAS}$ of dolostones is actually much higher, but that the CAS extraction leach steps failed to dissolve gypsum inclusions in the dolostones, leaving the gypsum to be dissolved during the acidification step. It has been suggested that leaching with DDIW is ineffective at dissolving gypsum, and that leaching with a 10% NaCl solution is more effective. However, because gypsum inclusions were very rare, it is unlikely that they would have been able to lower the observed $\delta^{34}S_{CAS}$ of dolostones by ~10 ‰ relative to limestone $\delta^{34}S_{CAS}$. Furthermore, the inability to effectively dissolve gypsum inclusions during CAS extraction does not address the lower $\delta^{34}S_{gypsum}$ values relative to limestone $\delta^{34}S_{CAS}$.

Assuming the $\delta^{34}S$ trends are not a laboratory artifact, one possible interpretation for the offset in $\delta^{34}S$ values is that the evaporites and the dolomitizing fluid formed in an evaporative setting where seawater was mixed with continentally-derived fluids; such fluids might contain ^{34}S-depleted sulfur phases resulting from the oxidative weathering of pyrite-rich shales (Kaufman et al., 2007). Evaporative concentration of Mg is common in such settings. The occurrence of more radiogenic $^{87}Sr/^{86}Sr$ values in some dolostones and gypstones supports this hypothesis, because continentally-derived fluids would contain ^{87}Rb that would decay to ^{87}Sr, and ultimately lead to more radiogenic $^{87}Sr/^{86}Sr$ values. Likewise, the trend of increasing $\delta^{18}O_{carb}$ with decreasing Ca/Mg (Fig. 5C) suggests that the dolomitizing fluid had experienced evaporation insofar as ^{18}O becomes preferentially enriched in water as evaporation progresses (e.g., Hoefs, 1997). However, it should be noted that the ^{18}O enrichment within the dolostones relative to the limestones (about +4‰) is similar to the expected $\delta^{18}O$ fractionation between dolomite and calcite precipitated from the same fluid (between +3‰ and +6‰), but it is difficult to demonstrate that the calcites and dolomites in question were precipitated from the same fluids (e.g., Tucker et al., 1990).

On the other hand, the depletion of ^{34}S in late-stage evaporite deposits has long been noted from ancient evaporite basins and has led previous workers to speculate that a Rayleigh-type distillation effect occurs as evaporite minerals are deposited (Nielsen and Ricke, 1964; Holser and Kaplan, 1966; Raab and Spiro, 1991). Assuming a fractionation between seawater and evaporite of 2‰ (e.g., Claypool et al., 1980), the $\delta^{34}S$ evolution of a hypothetical brine (starting at +35‰) and precipitate is shown as a function of fraction of fluid remaining in Fig. 7A. According to this ideal model, towards the end of the evaporation process, the $\delta^{34}S$ composition of the remaining fluid approaches 25‰, or 10‰ less than the starting fluid. Fig. 7B shows the isotopic difference between a brine and its initial isotopic composition as a function of evaporation at different fractionations between seawater and evaporite ($\Delta_{evaporite-seawater}$ of 1.6–2.4‰); it shows that regardless of the fractionation factor used, towards the end of evaporation, the remaining brine is depleted by more than 8‰ than the starting brine.

Deviations from the idealized Rayleigh distillation model have been reported from experimental work (e.g., Raab and Spiro, 1991), but for the present study, the ideal model does seem to fit the data. The high $\delta^{18}O$ values of dolostones relative to those of limestones would suggest that the dolomitizing fluid had experienced some degree of evaporative concentration. Likewise, the high $[SO_4]$ results also

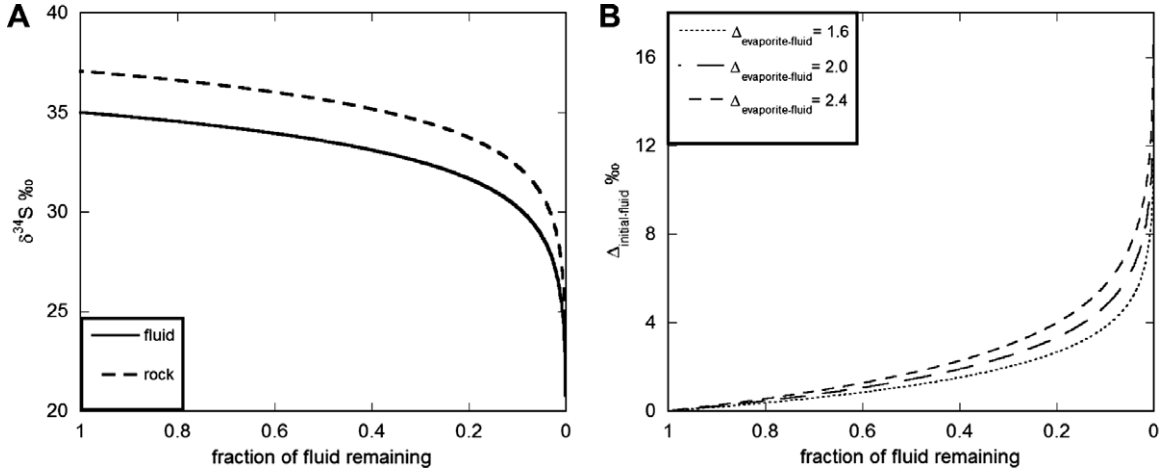

Fig. 7. Model results of Rayleigh-type ^{34}S depletion in a hypothetical brine and precipitate as evaporation progresses. (A) Graph shows $R_{fluid} = R_{initial} f^{\alpha-1}$ and $R_{rock} = \alpha R_{fluid}$ where R_{fluid} is the ratio ^{34}S:^{32}S in the fluid, $R_{initial}$ is the starting ratio ^{34}S:^{32}S in the fluid, R_{rock} is the ratio ^{34}S:^{32}S in the rock, f is the fraction of fluid remaining, and α is the fractionation factor between fluid and the precipitate, taken to be 1.002. Results are shown in the standard delta notation. (B) Graph shows $R_{initial} - R_{fluid}$ as a function of f at different values of α (1.0014, 1.002, and 1.0024). α values are shown as $\Delta_{evaporite-fluid}$ (1.6‰, 2.0‰, and 2.4‰).

suggest that highly evaporated seawater was the source of the dolomitizing fluid. In order to further explore this issue, a finer-scale sampling within the evaporite units is required, in addition to additional experimental investigation.

6.3. Hypothesis 3: $\delta^{34}S$ gradient with depth

An alternative interpretation of the $\delta^{34}S$ versus Ca/Mg results is that the CAS results are recording a primary seawater $\delta^{34}S_{sulfate}$ gradient with depth. The presence of a $\delta^{34}S_{sulfate}$ gradient in Early Triassic seas has been previously suggested (Newton et al., 2004; Kump et al., 2005; Riccardi et al., 2006; Marenco, 2007). The $\delta^{34}S$ equivalency between evaporite and dolostone, combined with marine strontium isotopic compositions in some dolostones (and only slightly more radiogenic values in others), and increased [CAS] in proximal dolostones could support this hypothesis.

A number of authors have suggested that the Permo-Triassic mass extinction may have been caused by shallow-ocean euxinia following a period of prolonged global deep-ocean anoxia (Isozaki, 1997; Newton et al., 2004; Grice et al., 2005; Kump et al., 2005; Riccardi et al., 2006; Marenco, 2007). During periods of extreme oceanic anoxia, deep ocean $\delta^{34}S$ would increase as sulfate concentrations decrease due to enhanced bacterial sulfate reduction in the water column. The oceanic sulfate pool would be split into an isotopically-enriched deep reservoir and an isotopically-depleted surface reservoir. The data presented here may provide evidence that anoxic conditions and a $\delta^{34}S$ gradient persisted at least until the end of the Spathian. However, it should be noted that in order to maintain a surface to deep gradient in oceanic sulfate $\delta^{34}S$ for millions of years, the oceanic sulfate pool would have to be considerably smaller than that of today (e.g., Marenco, 2007). Although this remains a possibility, the strong correlation between $\delta^{34}S_{CAS}$ and the degree of dolomitization makes a compelling case for dolomitization as the principle cause for the onshore–offshore trends in $\delta^{34}S_{CAS}$.

7. IMPLICATIONS FOR FUTURE CAS STUDIES

The results of this study have a number of important implications for the study of carbonate associated sulfate:

(1) The $\delta^{34}S$ of CAS in ancient rocks is robust against most diagenetic processes that would affect alteration indicators such as Mn/Sr and $^{87}Sr/^{86}Sr$. Lyons et al. (2004) concluded that the $\delta^{34}S_{CAS}$ of recent non-dolomitized sediments was independent of diagenetic processes; our results extend their conclusions to ancient rocks.

(2) The $\delta^{34}S$ of CAS in some basins may be altered during dolomitization, as indicated by a strong correlation between $\delta^{34}S_{CAS}$ and Ca/Mg. Although there may be multiple pathways for dolomitization to occur, the results presented here suggest that at least some dolostones in the rock record may contain altered $\delta^{34}S_{CAS}$ compositions relative to oceanic sulfate $\delta^{34}S$. There may be evidence to suggest that dolomitization mechanisms may have been different prior to the Phanerozoic (e.g., Corsetti et al., 2006); therefore, the effect of dolomitization on CAS in Precambrian rocks deserves further investigation.

(3) The mineral phase of choice for sulfur isotope chemostratigraphy is calcite (or aragonite, if available) from rocks formed in open, subtidal shelf settings. Because of the possibility of contamination with continentally-derived sources of ^{34}S-depleted sulfur and the potential for Rayleigh ^{34}S depletion during evaporation, evaporite deposits are less ideal for sulfur chemostratigraphy than subtidal shelf limestones. However, this finding requires supporting evidence from other basins throughout the rock record and thus warrants further study.

8. CONCLUSIONS

The results of this study indicate that there are significant variations in the $\delta^{34}S$ of CAS both within localities and between multiple localities from proximal evaporitic to distal subtidal environments. The variations in these broadly time-equivalent facies appear to be driven by the degree of dolomitization, as reflected in the Ca/Mg ratios of samples. Evaporites interbedded with dolostones exhibit similar $\delta^{34}S$ values to the CAS of dolostones. The close agreement in $\delta^{34}S$ between interbedded evaporite and dolostone suggests that either proximity to continentally-derived fluids with ^{34}S-depleted sulfur phases, evaporitic depletion of ^{34}S, or an Early Triassic $\delta^{34}S$ gradient with depth may have resulted in lower $\delta^{34}S$ in dolostones and evaporites relative to better preserved shallow subtidal limestones.

Given these diagenetic insights, the $\delta^{34}S$ composition of Spathian seawater sulfate may have been higher than previously thought. The $\delta^{34}S_{CAS}$ values from distal shelf limestones reported here suggest that Spathian seawater sulfate may have been between +31‰ and +38‰ VCDT, rather than the +25‰ to +30‰ values suggested by evaporite-based results (Fig. 3).

Analysis of CAS remains a powerful tool for the investigation of ancient seawater sulfate. However, as with any geochemical proxy, CAS results should be accompanied by diagenetic investigation, and where possible, paleoenvironmental analysis. Most importantly, the relationship between CAS and dolomitization should be further investigated in rocks from different basins and of different ages.

ACKNOWLEDGMENTS

We thank Isabel Montañez for invaluable assistance with thin-section staining techniques, Paul Marenco for field assistance, Will Berelson and Will Beaumont for help with organic carbon analyses. Reviews by Matthew Hurtgen, Tom Algeo, Timothy Lyons and an anonymous reviewer greatly improved an earlier version of this manuscript. This project was supported by the NSF (EAR 0447019) to Corsetti, Bottjer and Kaufman. Marenco was addi-

tionally supported with graduate student grants from the Geological Society of America, the American Association of Petroleum Geologists, the Paleontological Society, and the USC Department of Earth Sciences.

REFERENCES

Baud A., Atudorei V. and Sharp Z. (1996) Late Permian and Early Triassic evolution of the northern Indian margin; carbon isotope and sequence stratigraphy. *Geodin. Acta* **9**(2–3), 57–77.

Bissell H. J. (1970) Petrology and petrography of lower Triassic marine carbonates of southern Nevada (USA). In *International Sedimentary Petrographical Series*, vol. 14 (ed. H. M. E. Schuermann), p. 27.

Blakey R. C. (1974) Stratigraphic and depositional analysis of the Moenkopi formation, southeastern Utah. *Bull-Utah Geol. Miner. Surv.* **104**, 1–81.

Burchfiel B. C., Cameron C. S. and Royden L. H. (1997) Geology of the Wilson Cliffs-Potosi Mountain area, southern Nevada. *Int. Geol. Rev.* **39**(9), 830–854.

Burdett J. W., Arthur M. A. and Richardson M. (1989) A Neogene seawater sulfur isotope age curve from calcareous pelagic microfossils. *Earth Planet. Sci. Lett.* **94**(3–4), 189–198.

Claypool G. E., Holser W. T., Kaplan I. R., Sakai H. and Zak I. (1980) The age curves of sulfur and oxygen isotopes in marine sulfate and their mutual interpretation. *Chem. Geol.* **28**(3–4), 199–260.

Corsetti F. A., Baud A., Marenco P. J. and Richoz S. (2005) Summary of Early Triassic carbon isotope records. *C.R. Palevol.* **4**(6–7), 405–418.

Corsetti F. A., Kidder D. L. and Marenco P. J. (2006) Trends in oolite dolomitization across the Neproterozoic–Cambrian boundary: A case study from Death Valley, California. *Sediment. Geol.* **191**, 135–150.

Cortecci G., Reyes E., Berti G. and Casati P. (1981) Sulfur and oxygen isotopes in Italian marine sulfates of Permian and Triassic ages. *Chem. Geol.* **34**(1–2), 65–79.

Dickson J. A. D. (1966) Carbonate identification and genesis as revealed by staining. *J. Sediment. Petrol.* **36**(2), 491–505.

Gellatly A. M. and Lyons T. W. (2005) Trace sulfate in mid-Proterozoic carbonates and the sulfur isotope record of biospheric evolution. *Geochim. Cosmochim. Acta* **69**(15), 3813–3829.

Grassineau N. V., Mattey D. P. and Lowry D. (2001) Sulfur isotope analysis of sulfide and sulfate minerals by continuous flow-isotope ratio mass spectrometry. *Anal. Chem.* **73**, 220–225.

Grice K., Changqun C., Love G. D., Boettcher M. E., Twitchett R. J., Grosjean E., Summons R. E., Turgeon S. C., Dunning W. and Jin Y. (2005) Photic zone euxinia during the Permian-Triassic superanoxic event. *Science* **307**(5710), 706–709.

Hoefs J. (1997) *Stable Isotope Geochemistry*. Springer.

Holser W. T. (1984) Gradual and abrupt shifts in ocean chemistry during Phanerozoic time. In *Patterns Change Earth Evol.* (eds. H. D. Holland and A. F. Trendall). Springer-Verlag, pp. 123–143.

Holser W. T. and Kaplan I. R. (1966) Isotope geochemistry of sedimentary sulfates. *Chem. Geol.* **1**(2), 93–135.

Holser W. T. and Magaritz M. (1987) Events near the Permian–Triassic boundary. *Mod. Geol.* **11**(2), 155–180.

Holser W. T., Schidlowski M., Mackenzie F. T. and Maynard J. B. (1988) Geochemical cycles of carbon and sulfur. In *Chemical Cycles in the Evolution of the Earth* (eds. C. B. Gregor, R. M. Garrels, F. T. Mackenzie and J. B. Maynard). John Wiley and Sons, Inc., p. 276.

Hurtgen M. T., Arthur M. A., Suits N. S. and Kaufman A. J. (2002) The sulfur isotopic composition of Neoproterozoic seawater sulfate; implications for a snowball Earth? *Earth Planet. Sci. Lett.* **203**(1), 413–429.

Hurtgen M. T., Halverson G. P., Arthur M. A. and Hoffman P. F. (2006) Sulfur cycling in the aftermath of a 635-Ma snowball glaciation; evidence for a syn-glacial sulfidic deep ocean. *Earth Planet. Sci. Lett.* **245**(3–4), 551–570.

Isozaki Y. (1997) Permo–Triassic boundary superanoxia and stratified superocean; records from lost deep sea. *Science* **276**(5310), 235–238.

Kah L. C., Lyons T. W. and Frank T. D. (2004) Low marine sulphate and protracted oxygenation of the Proterozoic biosphere. *Nature* **431**, 834–837.

Kaiho K., Kajiwara Y., Nakano T., Miura Y., Kawahata H., Tazaki K., Ueshima M., Chen Z. and Shi G. R. (2001) End-Permian catastrophe by a bolide impact; evidence of a gigantic release of sulfur from the mantle. *Geology* **29**(9), 815–818.

Kampschulte A., Bruckschen P. and Strauss H. (2001) The sulphur isotopic composition of trace sulphates in Carboniferous brachiopods: implications for coeval seawater, correlation with other geochemical cycles and isotope stratigraphy. *Chem. Geol.* **175**, 165–189.

Kampschulte A. and Strauss H. (2004) The sulfur isotopic evolution of Phanerozoic seawater based on the analysis of structurally substituted sulfate in carbonates. *Chem. Geol.* **204**, 255–286.

Kaplan I. R., Emery K. O. and Rittenberg S. C. (1963) The distribution and isotopic abundance of sulphur in recent marine sediments off southern California. *Geochim. Cosmochim. Acta* **27**(4), 297–331.

Kaufman A. J., Corsetti F. A. and Varni M. A. (2007) The effect of rising atmospheric oxygen on carbon and sulfur isotope anomalies in the Neoproterozoic Johnnie Formation, Death Valley, USA. *Chem. Geol.* **237**, 47–63.

Korte C., Kozur H. W., Bruckschen P. and Veizer J. (2003) Strontium isotope evolution of Late Permian and Triassic seawater. *Geochim. Cosmochim. Acta* **67**(1), 47–62.

Kump L. R., Pavlov A. A. and Arthur M. A. (2005) Massive release of hydrogen sulfide to the surface ocean and atmosphere during intervals of oceanic anoxia. *Geology* **33**(5), 397–400.

Larson A. R. (1966) Stratigraphy and paleontology of Moenkopi Formation in southern Nevada. Doctoral, University of California Los Angeles.

Lyons T. W., Walter L. M., Gellatly A. M. and Marini A. M. (2004) Sites of anomalous organic remineralization in the carbonate sediments of South Florida, USA: the sulfur cycle and carbonate-associated sulfate. In *Microbial Sulfur Transformations Throughout Earth's History: Development, Changes, and Future of the Biogeochemical Sulfur Cycle: Geological Society of America Special Paper 379* (eds. J. Amend, K. Edwards and T. L.). Geological Society of America, pp. 161–176.

Marenco P. J. (2007) Sulfur isotope geochemistry and the End Permian mass extinction. Dissertation, University of Southern California.

McKee E. D. (1954) *Stratigraphy and History of the Moenkopi Formation of Triassic Age*. Geological Society of America (GSA).

Mekhtiyeva V. L. (1974) Sulfur isotopic composition of fossil molluscan shells as an indicator of hydrochemical conditions in ancient basins. *Geochem. Int.* **11**(6), 1188–1192.

Montanez I. P., Banner J. L., Osleger D. A., Borg L. E. and Bosserman P. J. (1996) Integrated Sr isotope variations and sea-level history of Middle to Upper Cambrian platform carbon-

ates; implications for the evolution of Cambrian seawater (super 87)Sr/(super 86)Sr. *Geology* **24**(10), 917–920.

Newton R., Pevitt P., Wignall P. B. and Bottrell S. (2004) Large shifts in the isotopic composition of seawater sulphate across the Permo–Triassic boundary in northern Italy. *Earth Planet. Sci. Lett.* **218**, 331–345.

Nielsen H. and Ricke W. (1964) Schwefel-isotopen verhältnisse von evaporiten aus deutschland; Ein beitrag zur kenntnis von δ34S im meerwasser-sulfat. *Geochim. Cosmochim. Acta* **28**, 577–591.

Payne J. L., Lehrmann D. J. W. J., Orchard M. J. S. D. P. and Knoll A. H. (2004) Large perturbations of the carbon cycle during recovery from the end-Permian extinction. *Science* **305**(5683), 506–509.

Paytan A., Kastner M., Campbell D. and Thiemens M. H. (1998) Sulfur isotopic composition of Cenozoic seawater sulfate. *Science* **282**(5393), 1459–1462.

Poborski S. J. (1954) Virgin Formation (Triassic) of the St. George, Utah, area. *GSA Bull.* **65**, 971–1006.

Raab M. and Spiro B. (1991) Sulfur isotopic variations during seawater evaporation with fractional crystallization. *Chem. Geol. Isot. Geosci. Sect.* **86**(4), 323–333.

Riccardi A. L., Arthur M. A. and Kump L. R. (2006) Sulfur isotopic evidence for chemocline upward excursions during the end-Permian mass extinction. *Geochim. Cosmochim. Acta* **70**, 5740–5752.

Strauss H. (1997) The isotopic composition of sedimentary sulfur through time. *Palaeogeogr. Palaeoclimatol. Palaeoecol.* **132**(1–4), 97–118.

Tucker M. E., Wright V. P. and Dickson J. A. D. (1990) *Carbonate Sedimentology*. Blackwell Publication.

Wilgus C. K. (1981) A stable isotope study of Permian and Triassic marine evaporite and carbonate rocks, Western Interior, USA. Doctoral, University of Oregon.

Associate editor: Frank Podosek